PAPER • OPEN ACCESS

Photon transport in one-dimensional systems coupled to three-level quantum impurities

To cite this article: Christoph Martens *et al* 2013 *New J. Phys.* **15** 083019

View the article online for updates and enhancements.

Photon transport in one-dimensional systems coupled to three-level quantum impurities

Christoph Martens[1,5]**, Paolo Longo**[2,3] **and Kurt Busch**[1,4]

[1] Max-Born-Institut, Max-Born-Strasse 2A, D-12489 Berlin, Germany
[2] Institut für Theoretische Festkörperphysik, Karlsruhe Institute of Technology (KIT), Wolfgang-Gaede-Strasse 1, D-76131 Karlsruhe, Germany
[3] Max-Planck-Institut für Kernphysik, Saupfercheckweg 1, D-69117 Heidelberg, Germany
[4] Humboldt-Universität zu Berlin, Institut für Physik, AG Theoretische Optik und Photonik, Newtonstrasse 15, D-12489 Berlin, Germany
E-mail: martens@mbi-berlin.de

Abstract. We discuss the transport properties of a single photon in a one-dimensional waveguide with an embedded three-level atom and utilize both stationary plane-wave solutions and time-dependent transport calculations to investigate the interaction of a photon with driven and undriven V- and Λ-systems. Specifically, for the case of an undriven V-system, we analyze the phenomenon of long-time occupation of the upper atomic levels in conjunction with *almost* dark states. For the undriven Λ-system, we find non-stationary dark states and we explain how the photon's transmittance can be controlled by an initial phase difference between the energetically lower-lying atomic states. With regard to the driven three-level systems, we discuss electromagnetically induced transparency in terms of the pulse propagation of a single photon through a Λ-type atom. In addition, we demonstrate how a driven V-type atom can be utilized to control the momentum distribution of the scattered photon.

[5] Author to whom any correspondence should be addressed.

IOP Institute of Physics · DEUTSCHE PHYSIKALISCHE GESELLSCHAFT

Contents

1. Introduction

Much of the recent progress in quantum photonics as well as in circuit and cavity quantum electrodynamics is based on considerable advances in micro- and nanofabrication techniques and on improvements in the understanding of the underlying physical mechanisms. Different approaches exist for the realization of quantum optical circuits, e.g. via superconducting devices [1, 2], semiconductor structures [3] or hybrid systems [4]. For instance, recent works have demonstrated the efficient coupling of quantum dots as single photon sources to the modes of integrated waveguiding elements [5] as well as the generation and manipulation of arbitrary one- and two-photon states in such systems [6].

Although the above approaches differ widely in materials and operating wavelenghts, their basic building blocks exhibit the same characteristics: they consist of low-dimensional waveguiding structures with embedded quantum impurities so that quantum interference can be utilized efficiently. From a theoretical vantage point, already the investigation of the apparently simple model of a single two-level system (2LS) embedded in a one-dimensional (1D) waveguide leads to interesting effects such as an energy-dependent mirror [7–10] or strong nonlinearities on the few-photon level [11–17]. In addition, it has recently been proposed to utilize these systems as local quantum probes within a Hong–Ou–Mandel setting [18].

These systems exhibit an even richer behavior (and associated level of complexity) if the 2LS is replaced by a three-level system (3LS). Already *stand-alone* 3LSs display interesting physical effects such as electromagnetically induced transparency (EIT) [19] and the possibility of adiabatic population transfer [20] that simply do not occur in 2LSs. EIT with classical radiation in the case of a single emitter embedded in a 1D system has been realized with the help of superconducting devices [21, 22]. Furthermore, 3LSs give the possibility to control and tune effects that do occur in 2LSs, but only in very specific situations that might be difficult to realize and/or maintain experimentally—the perfect mirror effect alluded to above being a case in point [23–25].

The stationary scattering properties of single- and two-photon plane-wave states in 1D waveguides with linearized dispersion relations and embedded driven and undriven 3LS have been analyzed recently [26–29]. Specifically, EIT for single photons and single atoms has been

described [27, 28], a proposal for a single-photon transistor has been formulated [27], and 3LS-mediated photon-bunching effects [28, 29] similar to the 2LS case [7, 8] have been found.

In this work, we give a detailed analysis of the scattering properties and dynamics of single-photon pulses that propagate in 1D waveguides with arbitrary (i.e. nonlinear) dispersion relations and interact with a single driven or undriven embedded 3LS. Specifically, we carry out analytical calculations for single-photon plane-wave states in the stationary regime and perform time-dependent simulations for single-photon pulses. The paper is organized as follows. We start with a description of the fundamentals in section 2. This is followed by sections 3 and 4, where we present the results of our work on undriven and driven V- and Λ-3LS, respectively. Specifically, we will see how a long-time occupation of upper atomic states can be reached, we consider the role of dark states in the undriven systems and how the relative phase of the atomic states can influence the single-photon scattering properties. In all these cases, we focus on the differences between the results of stationary plane-wave calculations and dynamical pulse–state simulations. In addition, we examine effects that result from the, in general, nonlinear dispersion relation of the waveguiding system. In section 5, we summarize our work and provide a brief outlook.

2. Fundamentals

We start by introducing the Hamiltonian of the above-described class of systems. Similar to other works [7–15, 27, 28], the Hamiltonian $\hat{H}$ consists of three parts:

$$\hat{H} = \hat{H}_W + \hat{H}_A + \hat{H}_I. \tag{1}$$

Here, $\hat{H}_W$ represents a 1D waveguide for which we assume a tight-binding model that describes the quantized modes of the waveguide on an equidistant real-space lattice (lattice spacing $a = 1$) with nearest neighbor coupling J ($\hbar = 1$):

$$\hat{H}_W = \sum_x \omega_0 \, \hat{a}_x^\dagger \hat{a}_x - J \sum_x \left(\hat{a}_x^\dagger \hat{a}_{x+1} + \hat{a}_{x+1}^\dagger \hat{a}_x \right). \tag{2}$$

The operators $\hat{a}_x^\dagger$ and $\hat{a}_x$ denote the bosonic creation and annihilation operators for photons at site x of the waveguide. The first term of Hamiltonian (2) represents the photonic on-site energy ω_0, i.e. the eigenenergy of an uncoupled site. The second term describes the hopping between neighboring sites with strength J. Such a model features one band with a cosine-shaped dispersion relation $\epsilon_k = \omega_0 - 2J \cos(k)$ that is generic in the sense that it exhibits approximately linear dispersion near the center of the band and features band edges (cut-off frequencies) where the dispersion relation is approximately quadratic and a slow-light regime is formed. Both features are characteristic of a number of physical systems such as mono-mode fibers, ridge waveguides and coupled-resonator as well as photonic crystal waveguides. The latter two systems correspond particularly well to a tight-binding model. Clearly, systems with more than one band and different dispersion relations can be modeled by going beyond the nearest-neighbor interaction. For instance, in the case of photonic crystals this is facilitated by a Wannier function approach [30]. Such models allow for the quantitative descriptions of realistic systems via the same numerical methods that we use below, but such models considerably complicate the analytical treatment without changing the qualitative features. At this point, we would like to note that several of the works mentioned above [7, 8, 11–13, 27, 28] utilize linearized dispersion
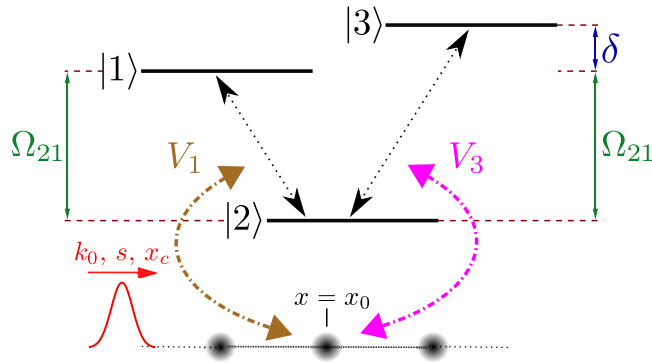
Figure 1. The V-system consists of the ground state $|2\rangle$ and the two upper states $|1\rangle$ and $|3\rangle$. The transition energy between $|2\rangle$ and $|3\rangle$ is detuned by δ with respect to the transition energy between $|2\rangle$ and $|1\rangle$, denoted by Ω_{21}. The waveguide mode couples from site x_0 to the two atomic transitions with the strengths V_1 and V_3. The initial single-photon state is a Gaussian wave packet with width s, carrier wavenumber k_0 and is centered around x_c.

relations, which are extended to infinity, i.e. the physics associated with slow-light regimes, band edges and band gaps has not been discussed in these works.

States of natural atoms have well-defined parities, and radiative dipole transitions are only allowed between states of different parity. Therefore, exactly one of the three transitions of a 3LS is dipole-forbidden. Consequently, one distinguishes between three configurations, the so-called V-, Λ- and ladder configurations. In the V-configuration, a single ground-state dipole couples to two excited states, which themselves do not couple (see figure 1). Conversely, in the Λ-configuration, two energetically lower lying states dipole couple to one common excited state (see figure 4). In the ladder-configuration, a ground-state dipole couples to an energetically intermediate state that in turn dipole couples to an energetically higher-lying state. The corresponding Hamiltonians $\hat{H}_A$ will be specified in the respective subsections that deal with driven and undriven 3LS. In the context of single-photon transport the ladder-configuration is considerably less important, since in the undriven case and in the single excitation regime (see below, equation (4)) the highest level is irrelevant and the physics is the same as for a 2LS consisting of the two lower states of the ladder system. The driven cases of ladder systems are equivalent to the driven V- and Λ-systems. Therefore, we will, in the following, not consider the ladder system.

As a result, the Hamiltonians $\hat{H}_I$, which describe the interaction of the waveguide modes with the (yet to be specified) 3LS are of the form

$$\hat{H}_I = \sum_{l=\alpha,\beta} V_l \left(|l_\uparrow\rangle\langle l_\downarrow| \, \hat{a}_{x_0} + \text{h.c.} \right). \tag{3}$$

The sum in (3) runs over the two dipole-allowed transitions denoted by α and β. The states $|l_\downarrow\rangle$ and $|l_\uparrow\rangle$ represent the lower and upper states of the transition l, respectively. The coupling strengths to the waveguide modes are given by V_l. For simplicity, we assume that the coupling constants are independent of the wavenumber k, so that we obtain a local coupling of the 3LS to a single waveguide site x_0 (cf the above discussion regarding the use of a tight-binding model for the waveguide).

The full Hamiltonian (1) commutes with the total number of excitations

$$\hat{C} = \sum_x \hat{a}_x^\dagger \hat{a}_x + \sum_{\gamma_\uparrow} |\gamma_\uparrow\rangle\langle\gamma_\uparrow|. \tag{4}$$

As a result, the Hilbert space associated with the system waveguide+3LS may be decomposed into subspaces of conserved excitation number. In turn, this facilitates the utilization of exact numerics as described below.

The second sum in (4) runs over all *upper* states $|\gamma_\uparrow\rangle$ of the impurity. In this work, we restrict ourselves to the transport of single photons through the waveguide+3LS system, so that $\langle\hat{C}(t)\rangle = 1 \,\forall\, t$. The most general single excitation state $|\Phi(t)\rangle$ of our system reads

$$|\Phi(t)\rangle = \sum_{x,\,\xi_\downarrow} g_{x,\,\xi_\downarrow}(t)\, \hat{a}_x^\dagger |0,\xi_\downarrow\rangle + \sum_{\gamma_\uparrow} s_{\gamma_\uparrow}(t)\, |0,\gamma_\uparrow\rangle, \tag{5}$$

where the first sum runs over all waveguide sites x and over the lower state(s) $|\xi_\downarrow\rangle$ of the 3LS. We denote the corresponding photon occupation amplitudes of the waveguide sites x by $g_{x,\,\xi_\downarrow}(t)$. Further, we denote with $s_{\gamma_\uparrow}(t)$ the occupation amplitude(s) of the upper impurity state(s) $|\gamma_\uparrow\rangle$ and there is no photon in the waveguide.

For dynamical transport calculations, we evolve an initial quantum state $|\Psi(t_0)\rangle$ in time according to

$$|\Psi(t)\rangle = \exp(-\mathrm{i}\,\hat{H}\,(t - t_0))|\Psi(t_0)\rangle. \tag{6}$$

In particular, we utilize a Krylov-subspace-based operator-exponential techniques [10, 14, 15]. In the following, we will exclusively work with initial states without the excitation of the upper atomic level(s), i.e. $s_{\gamma_\uparrow}(t_0) = 0$ in (5). For the initial photon amplitudes $g_{x,\,\xi_\downarrow}(t_0)$ we employ a normalized Gaussian wave packet in one or two of the subspaces associated with the lower state(s) of the impurity. Observables for transmittance, reflectance and occupation of the atomic states are defined in analogy to earlier works [10, 14, 15].

3. Single-photon transport through undriven three-level system

We investigate the scattering of single photons by a 3LS that is coupled to a waveguide. To this end, we employ analytical calculations for stationary situations involving plane wave states (cf [9, 27]) and compare with numerical analyses that focus on the dynamical features of the systems (using the time-evolution technique described above, cf [10, 14, 15]).

3.1. Long-time occupation in an undriven V-system

The atomic Hamiltonian $\hat{H}_A$ and the interaction Hamiltonian $\hat{H}_I$ for an undriven V-system read, respectively, as

$$\hat{H}_A = (E_2 + \Omega_{21})\, |1\rangle\langle1| + E_2\, |2\rangle\langle2| + (E_2 + \Omega_{21} + \delta)\, |3\rangle\langle3|, \tag{7}$$

$$\hat{H}_I = \sum_{i=1,3} V_i \left(|i\rangle\langle2|\hat{a}_{x_0} + \text{h.c.} \right). \tag{8}$$

Consequently, a general single-excitation state $|\Phi(t)\rangle$ and the initial state $|\Psi(t_0)\rangle$ for an incoming single photon read, respectively, as

$$|\Phi(t)\rangle = \sum_x g_x(t)\, \hat{a}_x^\dagger |0,2\rangle + s_1(t)\, |0,1\rangle + s_3(t)\, |0,3\rangle, \tag{9}$$
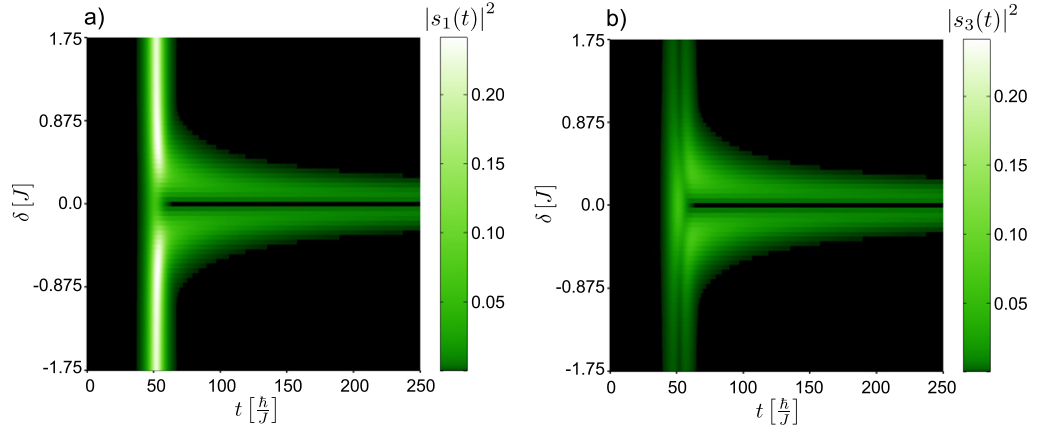
Figure 2. Occupation of the upper atomic states $|1\rangle$ (panel (a)) and $|3\rangle$ (panel (b)) for a simulation of a single-photon pulse of the form (10). The occupation is shown as a function of the simulation time t and the detuning δ of the two atomic transitions. Note the long-time occupation for small values of the detuning δ. The parameters of the simulation are $V_1 = V_3 = J$, $\Omega_{21} = \epsilon_{k_0}$, $\omega_0 = 0$, $k_0 = \pi/2$, $s = 9$, $x_c = 400$, and the waveguide has an extent of 999 real-space sites.

$$|\Psi(t_0)\rangle = \sum_x \phi_x^{k_0,x_c,s}\, \hat{a}_x^\dagger |0,2\rangle. \qquad (10)$$

Here, the Gaussian wave packet $\phi_x^{k_0,x_c,s} \propto \exp(-(x-x_c)^2/(2s^2) + \mathrm{i}\,k_0 x)$ of width s and which is centered at x_c is launched with wave vector k_0 (corresponding to the photon energy ϵ_{k_0}; see also figure 1).

In figure 2, we display the occupation of the two upper atomic levels as a function of the simulation time t and the detuning δ, when the atomic transition is on resonance, i.e. $\Omega_{21} = \epsilon_{k_0}$. In these plots, pronounced tails occur and this indicates a long-time occupation of the upper levels. Numerical diagonalizations have revealed that this effect arises from the excitation of *almost* dark states, i.e. states with a high occupation of the upper atomic states and a very low but non-vanishing occupation of the waveguide. Such states are eigenstates of systems whose detuning δ is small but non-zero and where the carrier wavenumber's energy is on resonance with one of the two transitions. These characteristics can be understood as follows.

Inserting (9) into the time-dependent Schrödinger equation leads to the following equations of motion (we set $E_2 = 0$ and $x_0 = 0$ for simplicity):

$$\mathrm{i}\frac{\partial}{\partial t} g_x(t) = -J\,(g_{x-1}(t) + g_{x+1}(t)) + \omega_0\, g_x(t) + V_1\, s_1(t)\,\delta_{x0} + V_3\, s_3(t)\,\delta_{x0}, \qquad (11a)$$

$$\mathrm{i}\frac{\partial}{\partial t} s_1(t) = \Omega_{21}\, s_1(t) + V_1\, g_0(t), \qquad (11b)$$

$$\mathrm{i}\frac{\partial}{\partial t} s_3(t) = (\Omega_{21} + \delta)\, s_3(t) + V_3\, g_0(t). \qquad (11c)$$

Almost dark states correspond to the situation where the emission of the atom into the waveguide is *slow*. We assume no initial occupation in the waveguide, i.e.

$$g_x(t_0) = 0 \quad \forall\, x, \qquad (12)$$

and a slowly varying amplitude g_0, i.e. $[|\partial/\partial t\, g_0(t)|]_{t=t_0} \ll |J|$. With the help of (11a), it then follows that

$$s_1(t_0) \approx -\frac{V_3}{V_1}\, s_3(t_0)\,. \tag{13}$$

Inserting (13) into (11b) finally leads to

$$\Omega_{21}\, s_3(t_0) \approx \left[\mathrm{i}\frac{\partial}{\partial t}s_3(t)\right]_{t=t_0} = (\Omega_{21} + \delta)\, s_3(t_0)\,, \tag{14a}$$

$$\Rightarrow \Omega_{21} \approx (\Omega_{21} + \delta) \Rightarrow |\delta| \ll |\Omega_{21}|. \tag{14b}$$

In other words, the emission of radiation from the atom into the waveguide is slow if the amplitudes of the upper atomic states follow (13) and if the detuning δ is almost vanishing. The first condition depends on the amplitudes and the relative phase of the upper atomic levels. The second condition is exactly the one mentioned above for which these almost dark states occur.

In the above argumentation, we did not allude to the amplitudes $g_{x \neq x_0}(t)$. If the atom radiates into the waveguide, the sites at $x \neq x_0$ transport the radiation away from the atom. Effectively, these sites form a loss channel of a cavity (site x_0) to which the atom is coupled. In this picture, a similar long-time occupation effect should occur in a *poor man's model* of a single 3LS interacting with a single mode of a leaky cavity. In this model, losses can be modeled by a negative imaginary part of the cavity's on-site energy. In the equations of motions (11a)–(11c) the waveguide part can then be formally replaced by

$$-J\,(g_{x-1}(t) + g_{x+1}(t)) + \omega_0\, g_x(t) \to (\mathrm{Re}(\omega_c) + \mathrm{i}\mathrm{Im}(\omega_c))\, g_c(t)\,, \tag{15}$$

and we arrive at the *poor man's model*. Here, ω_c denotes the cavity's on-site energy. A general single-excitation state $|\Theta(t)\rangle$ of this system is of the form

$$|\Theta(t)\rangle = g_c(t)\, \hat{a}_c^\dagger|0, 2\rangle + s_{c,1}(t)\, |0, 1\rangle + s_{c,3}(t)\, |0, 3\rangle. \tag{16}$$

In figure 3, we display the occupation of the upper atomic levels in our poor man's model for the same parameter ranges as in figure 2. In these simulations, the single excitation initially occupied the cavity mode and the atom was in its ground state, i.e. $g_c(t_0) = 1$ and $s_{c,1}(t_0) = s_{c,3}(t_0) = 0$ in (16). As expected, the characteristic tails associated with long-time occupations can be recovered qualitatively by our effective poor man's model system.

3.2. Non-stationary dark states and phase-dependent scattering by an undriven Λ-system

The Hamiltonian $\hat{H}_A$ for the free and undriven Λ-system reads

$$\hat{H}_A = E_1|1\rangle\langle 1| + (E_1 + \Omega_{12})\,|2\rangle\langle 2| + (E_1 - \delta)\,|3\rangle\langle 3|, \tag{17}$$

while the interaction $\hat{H}_I$ of the waveguide modes with the atom is modeled by

$$\hat{H}_I = \sum_{i=1,3} V_i\,(|2\rangle\langle i|\hat{a}_{x_0} + \mathrm{h.c.}), \tag{18}$$

and a general single-excitation state in this system is of the form

$$|\Phi(t)\rangle = \sum_x \left(g_{1,x}(t)\, \hat{a}_x^\dagger|0, 1\rangle + g_{3,x}(t)\, \hat{a}_x^\dagger|0, 3\rangle\right) + s_2(t)\, |0, 2\rangle. \tag{19}$$
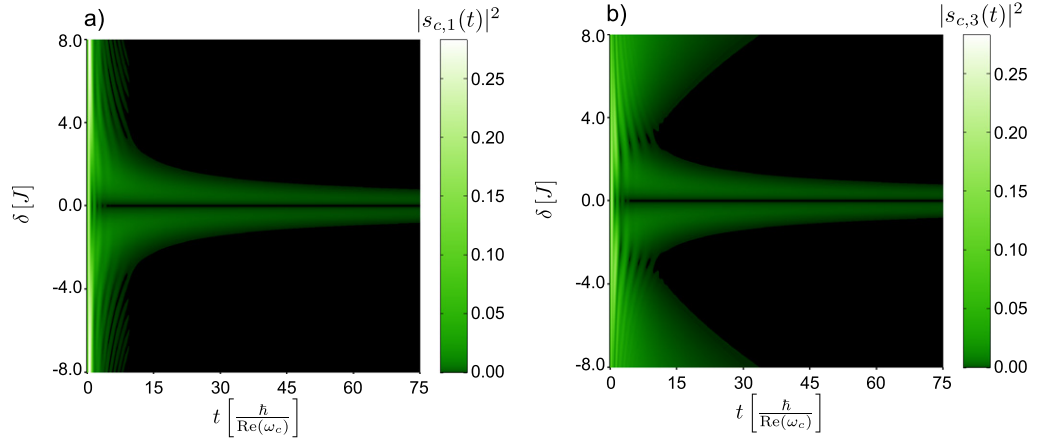
Figure 3. Occupation of the upper atomic states $|1\rangle$ (panel (a)) and $|3\rangle$ (panel (b)) for the simulation of a V-type three-level atom, which is coupled to a leaky single-mode cavity in the regime of a single excitation. The long-time occupation can occur in such systems, too. See text for further details. The parameters of the simulations are $V_1 = V_3 = 2\,\mathrm{Re}(\omega_c)$, $E_1 = \mathrm{Re}(\omega_c)$, $\mathrm{Im}(\omega_c) = -2$.

The undriven Λ-system thus exhibits two energetically lower states, $|1\rangle$ and $|2\rangle$. From each of these states the absorption of photons in conjunction with the transition to a (common) higher state $|2\rangle$ is possible. The details depend on the initial state of the atom and we consider here two possibilities. First, we look at the one-channel case (OCC), whereby the atom is initially in one of the lower states, e.g. without the loss of generality, in state $|1\rangle$. For this OCC, we use the initial state

$$|\Psi_{\mathrm{OCC}}(t_0)\rangle = \sum_x \phi_x^{k_0, x_c, s}\, \hat{a}_x^\dagger |0, 1\rangle. \tag{20}$$

The second class of initial states we consider here is that of a coherent superposition of the two lower atomic states—the two-channel case (TCC). The corresponding initial states read

$$|\Psi_{\mathrm{TCC}}(t_0)\rangle = \sum_x \phi_x^{k_0, x_c, s} \left(\hat{a}_x^\dagger |0, 1\rangle + \mathrm{e}^{\mathrm{i}\Delta\varphi} \hat{a}_x^\dagger |0, 3\rangle \right). \tag{21}$$

Here, the relative phase $\exp(\mathrm{i}\Delta\varphi)$ between the two lower atomic states is a new and, as we shall show below, important parameter. The setup of the corresponding simulations is shown in figure 4.

As usual, inserting (19) into the time-dependent Schrödinger equation leads to the equations of motion for this system ($E_1 = 0$, $x_0 = 0$):

$$\mathrm{i}\frac{\partial}{\partial t} g_{1,x}(t) = -J \left(g_{1,x-1}(t) + g_{1,x+1}(t) \right) + (E_1 + \omega_0)\, g_{1,x}(t) + V_1\, s_2(t)\, \delta_{x0}, \tag{22a}$$

$$\mathrm{i}\frac{\partial}{\partial t} g_{3,x}(t) = -J \left(g_{3,x-1}(t) + g_{3,x+1}(t) \right) + (E_1 - \delta + \omega_0)\, g_{3,x}(t) + V_3\, s_2(t)\, \delta_{x0}, \tag{22b}$$

$$\mathrm{i}\frac{\partial}{\partial t} s_2(t) = (E_1 + \Omega_{12})\, s_2(t) + V_1\, g_{1,0} + V_3\, g_{3,0}(t). \tag{22c}$$

With the help of (22a) and (22b) we can interpret the two cases OCC and TCC as a photonic excitation in our waveguide, while the Λ-atom is in one of its lower states. We will denote this as the photon being in the channel i, where i indicates the lower atomic state $|i\rangle$.
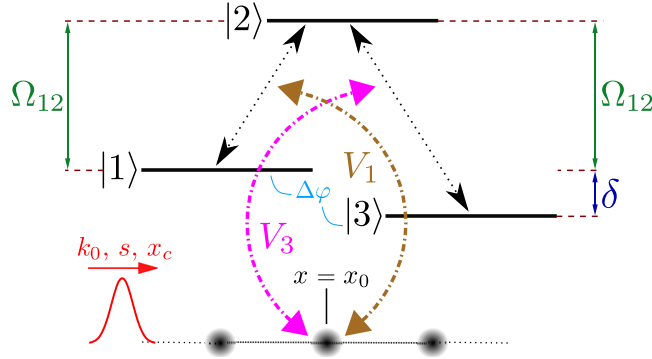
Figure 4. Illustration of waveguiding systems with a side coupled Λ-system. The notations are essentially the same as in figure 1. The only new parameter here is the relative phase $\Delta\varphi$ between the two lower atomic states.

3.2.1. Non-stationary dark states. In a dark state, the upper atomic state $|2\rangle$ will always be unoccupied, i.e. $\frac{\partial}{\partial t} s_2(t) = s_2(t) = 0 \, \forall \, t$. With the help of (22c), this leads to $g_{1,0} = -V_3/V_1 \, g_{3,0}$ and, by employing (22b) and (22a), we obtain

$$\delta \, g_{1,0}(t) = -J \left(g_{1,1}(t) + g_{1,-1}(t) + \frac{V_3}{V_1} \left(g_{3,1}(t) + g_{3,-1}(t) \right) \right), \tag{23a}$$

$$\delta \, g_{3,0}(t) = -J \left(\frac{V_1}{V_3} \left(g_{1,1}(t) + g_{1,-1}(t) \right) + g_{3,1}(t) + g_{3,-1}(t) \right). \tag{23b}$$

As a result, different types of dark states can exist in this system, not only stationary ones. Assuming zero detuning, i.e. $\delta = 0$, we infer

$$g_{1,1}(t) = -\frac{V_3}{V_1} g_{3,1}(t), \tag{24a}$$

$$g_{1,-1}(t) = -\frac{V_3}{V_1} g_{3,-1}(t), \tag{24b}$$

and with the help of (22a) and (22b), we have

$$g_{1,i}(t) = -\frac{V_3}{V_1} g_{3,i}(t). \tag{25}$$

If the coupling of the waveguide to both atomic transitions is equal, i.e. $V_1 = V_3$ and $\Delta\varphi = \pi$, the system is in a non-stationary dark state. An example for this case is shown in figure 5.

3.2.2. Phase dependence in the degenerate case. The above raises questions regarding the properties of stationary scattering solutions. As usual, we employ a time-harmonic ansatz for (22a)–(22c)

$$s_2(t) = \exp\left(-\mathrm{i}E_k t\right) v_3, \quad g_{i,x}(t) = \exp\left(-\mathrm{i}E_k t\right) w_{j,x}, \quad j \in \{1, 3\}, \tag{26}$$

where E_k represents the eigenenergy of a stationary solution. The amplitude $w_{j,x}$ describes an excitation of the waveguide site x in channel j, i.e. in the subspace of the atomic state $|j\rangle$.
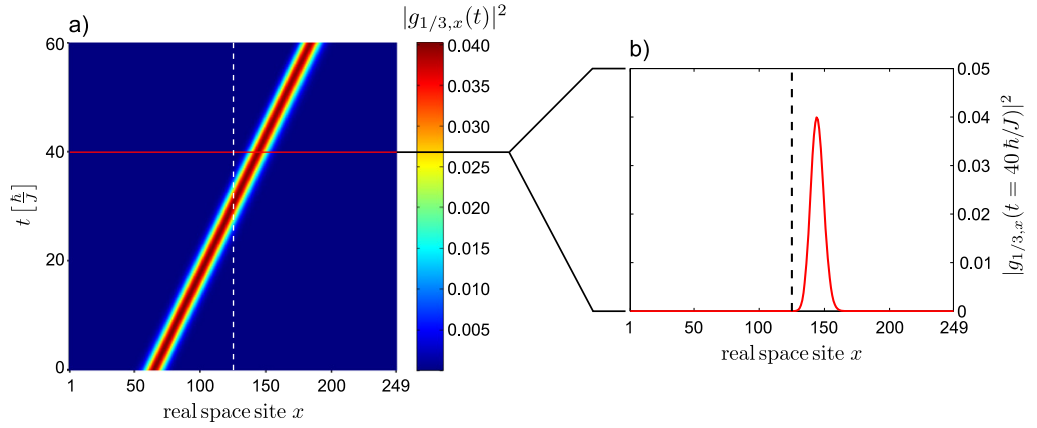
Figure 5. Occupation of the waveguide sites as a function of time (panel (a)) and a snapshot (panel (b)) when the photon has completely passed the waveguide site to which the three-level quantum impurity is side coupled to (indicated by a dashed line). The figure displays only one of the two channels since the occupation is identical in both. The wave packet is transmitted completely, i.e. the system is in a non-stationary dark state, although the photon energy ϵ_{k_0} is on resonance with the transition energy Ω_{12}. The parameters of the simulation are $\Delta\varphi = \pi$, $V_1 = V_3 = J$, $\Omega_{12} = \epsilon_{k_0}$, $\delta = 0$, $k_0 = \pi/2$, $s = 7$, $x_c = 65$, and the waveguide consists of 249 real-space sites.

To arrive at the stationary scattering solutions for a TCC, we make the ansatz

$$w_{1,x} = \begin{cases} \dfrac{1}{\sqrt{2}}\,\mathrm{e}^{\mathrm{i}k_{11}x} + r_{11}\,\mathrm{e}^{-\mathrm{i}k_{11}x} + t_{13}\,\mathrm{e}^{-\mathrm{i}k_{13}x}, & \text{for } j < 0, \\[2mm] t_{11}\,\mathrm{e}^{\mathrm{i}k_{11}x} + t_{13}\,\mathrm{e}^{\mathrm{i}k_{13}x}, & \text{for } j > 0, \end{cases} \tag{27a}$$

$$w_{3,x} = \begin{cases} \dfrac{\mathrm{e}^{\mathrm{i}\Delta\varphi}}{\sqrt{2}}\,\mathrm{e}^{\mathrm{i}k_{33}x} + r_{33}\,\mathrm{e}^{-\mathrm{i}k_{33}x} + t_{31}\,\mathrm{e}^{-\mathrm{i}k_{31}x}, & \text{for } j < 0, \\[2mm] t_{33}\,\mathrm{e}^{\mathrm{i}k_{33}x} + t_{31}\,\mathrm{e}^{\mathrm{i}k_{31}x}, & \text{for } j > 0. \end{cases} \tag{27b}$$

The physical meaning of the above equations is the following: in both channels, there are left-moving plane waves with wavenumbers k_{11} and k_{33}, respectively, that are incident upon the atom. Although these plane waves are parts of the wavefunction of the same photon, their stationary scattering process can be treated as a superposition of two independent OCCs. Specifically, the incoming plane wave in channel 1, i.e. $1/\sqrt{2}\,\mathrm{e}^{\mathrm{i}k_{11}x}$, is scattered by the Λ-system into a reflected and a transmitted part in channel 1 ($r_{11}\,\mathrm{e}^{-\mathrm{i}k_{11}x}$ and $t_{11}\,\mathrm{e}^{\mathrm{i}k_{11}x}$ in (27a)) and into a reflected and a transmitted part in channel 3 ($t_{31}\,\mathrm{e}^{\mathrm{i}k_{31}x}$ and $t_{31}\,\mathrm{e}^{-\mathrm{i}k_{31}x}$ in (27b)). By the same token, the incoming plane wave in channel 3, i.e. $\mathrm{e}^{\mathrm{i}\Delta\varphi}/\sqrt{2}\,\mathrm{e}^{\mathrm{i}k_{33}x}$, is similarly scattered into both channels (channel 3: $r_{33}\,\mathrm{e}^{-\mathrm{i}k_{33}x}$ and $t_{33}\,\mathrm{e}^{\mathrm{i}k_{33}x}$ in (27b), channel 1: $t_{13}\,\mathrm{e}^{\mathrm{i}k_{13}x}$ and $t_{13}\,\mathrm{e}^{-\mathrm{i}k_{13}x}$ in (27a)).

The wavenumbers in each of the distinct scattering process above are related via

$$\cos(k_{31}) = \cos(k_{11}) - \frac{\delta}{2J}, \tag{28a}$$

$$\cos(k_{13}) = \cos(k_{33}) + \frac{\delta}{2J}, \tag{28b}$$

due to the conservation of energy. Therefore, in the degenerate system with $\delta = 0$, we have $k_{31} = k_{11}$ and $k_{13} = k_{33}$. The wavenumbers k_{11} and k_{33}, which correspond to the incoming photon, are independent of each other and can be regarded as free parameters. Physically, if their values differ, it would mean that the wave function of the photon is a superposition of different momenta in the two atomic subspaces.

Now, we assume that before any interaction of the photon and the atom takes place, the combined system of waveguide and atom is in a product state of waveguide modes with atomic states. In this case, the wavenumbers that describe the incoming photon cannot be different for the two atomic subspaces, i.e. we have

$$k_{11} = k_{31} = k_{33} = k_{13} = k. \tag{29}$$

Under these conditions our ansatz reads

$$w_{1,x} = \begin{cases} \dfrac{1}{\sqrt{2}}\,\mathrm{e}^{\mathrm{i}kx} + r_{k1}\,\mathrm{e}^{-\mathrm{i}k_x}, & j < 0, \\[2mm] t_{k1}\,\mathrm{e}^{\mathrm{i}kx}, & j > 0, \end{cases} \tag{30a}$$

$$w_{3,x} = \begin{cases} \dfrac{\mathrm{e}^{\mathrm{i}\Delta\varphi}}{\sqrt{2}}\,\mathrm{e}^{\mathrm{i}kx} + r_{k3}\,\mathrm{e}^{-\mathrm{i}kx}, & j < 0, \\[2mm] t_{k3}\,\mathrm{e}^{\mathrm{i}kx}, & j > 0, \end{cases} \tag{30b}$$

with

$$r_{k1} = r_{11} + t_{13}, \tag{31a}$$

$$t_{k1} = t_{11} + t_{13}, \tag{31b}$$

$$r_{k3} = r_{33} + t_{31}, \tag{31c}$$

$$t_{k3} = t_{33} + t_{31}. \tag{31d}$$

Inserting (30a) and (30b) together with (26) into (22a)–(22c), we obtain

$$r_{k1} = \frac{-V_1\,(V_1 + \exp(\mathrm{i}\Delta\varphi))\,V_3)}{\sqrt{2}\left(V_1^2 + V_3^2 + 2\mathrm{i}J\,(\Omega_{12} - \epsilon_k)\sin(k)\right)}, \tag{32a}$$

$$t_{k1} = \frac{V_3\,(V_3 - \exp(\mathrm{i}\Delta\varphi)\,V_1) + 2\mathrm{i}J\,(\Omega_{12} - \epsilon_k)\sin(k)}{\sqrt{2}\left(V_1^2 + V_3^2 + 2\mathrm{i}J\,(\Omega_{12} - \epsilon_k)\sin(k)\right)}, \tag{32b}$$

$$r_{k3} = \frac{-V_3\,(V_1 + \exp(\mathrm{i}\Delta\varphi))\,V_3)}{\sqrt{2}\left(V_1^2 + V_3^2 + 2\mathrm{i}J\,(\Omega_{12} - \epsilon_k)\sin(k)\right)}, \tag{32c}$$

$$t_{k3} = \frac{V_1\,(\exp(\mathrm{i}\Delta\varphi)\,V_1 - V_3) + 2\mathrm{i}J\,\exp(\mathrm{i}\Delta\varphi)\,(\Omega_{12} - \epsilon_k)\sin(k)}{\sqrt{2}\left(V_1^2 + V_3^2 + 2\mathrm{i}J\,(\Omega_{12} - \epsilon_k)\sin(k)\right)}. \tag{32d}$$

The physical interpretation of these coefficients is as follows. Initially, we have a degenerate Λ-atom in an equal superposition of its lower states, i.e.

$$|\mathrm{atom}\rangle_{\mathrm{initial}} = \frac{1}{\sqrt{2}}\left(|1\rangle + \exp(\mathrm{i}\Delta\varphi)\,|3\rangle\right). \tag{33}$$
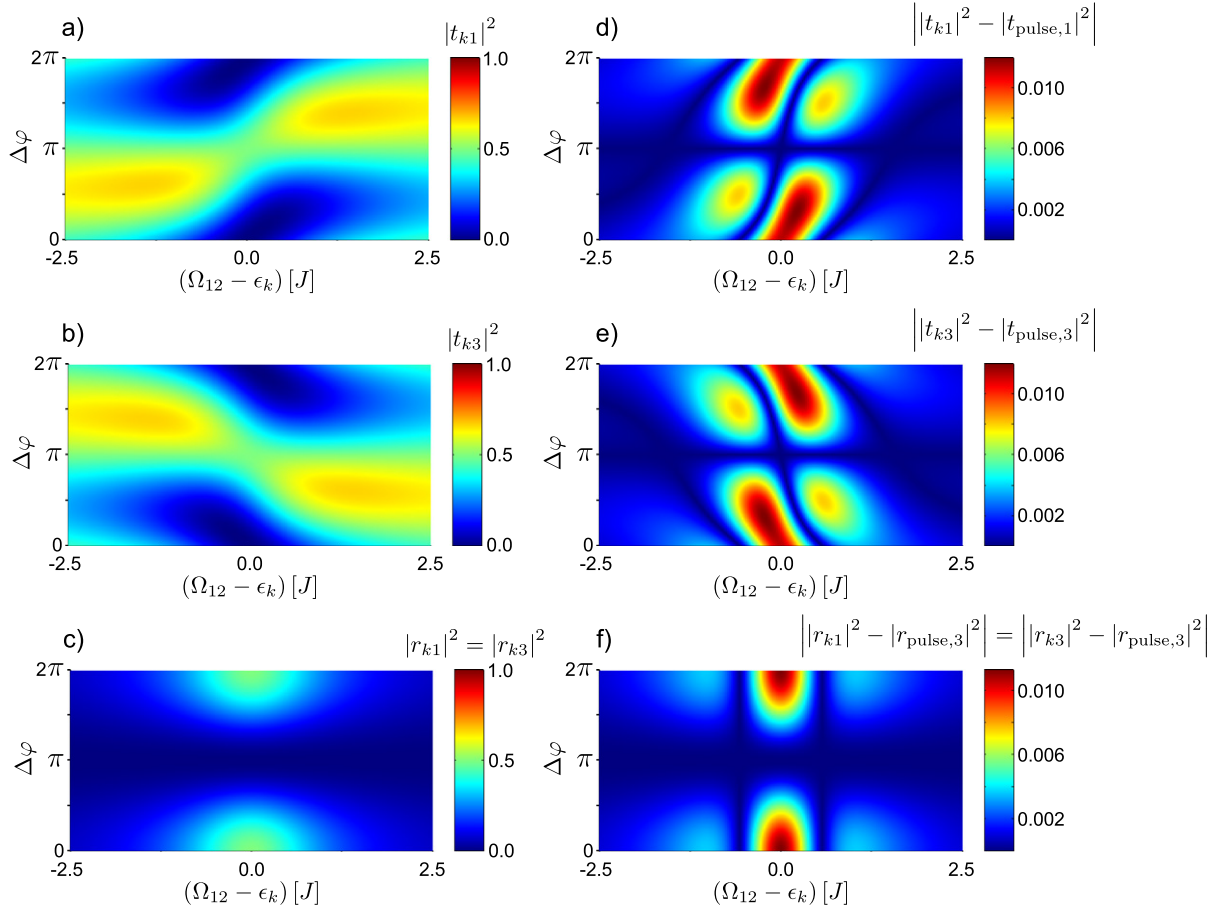
Figure 6. The degenerate Λ-system for TCC initial conditions: calculated transmittance in channel 1 (panel (a)), channel 3 (panel (b)) and calculated reflectance in both channels (panel (c)) as a function of the relative phase $\Delta\varphi$ and the detuning between the photon energy ϵ_k and the transition energy Ω_{12}. In contrast to the transmittances, the reflectances in each channel are identical for all parameters. Panels (d)–(f) show the absolute difference of the analytical stationary solutions and the results of time-dependent simulations for Gaussian pulses as described in figure 5. For $\Delta\varphi = \pi$, this difference vanishes completely. This situation corresponds to the case of time-dependent dark states mentioned in the text. Generally, the simulated results for the transmittances and the reflectances differ due to the finite width in momentum space of the pulse. The parameters of the simulation are $V_1 = V_3 = J$, $\Omega_{12} = 0$, $\delta = 0$, $k_0 = \pi/2$, $s = 9$, $x_c = 85$ and the waveguide consists of 299 real-space sites.

Then, a single photon with wavenumber k is scattered by the atom. After the scattering, we detect the photon as either being reflected or transmitted. In the first case, the state of the atom after scattering is

$$|\text{atom}\rangle_{\text{photon reflected}} = r_{k1}|1\rangle + r_{k3}|3\rangle. \tag{34}$$

In the second case, the state of the atom after scattering is

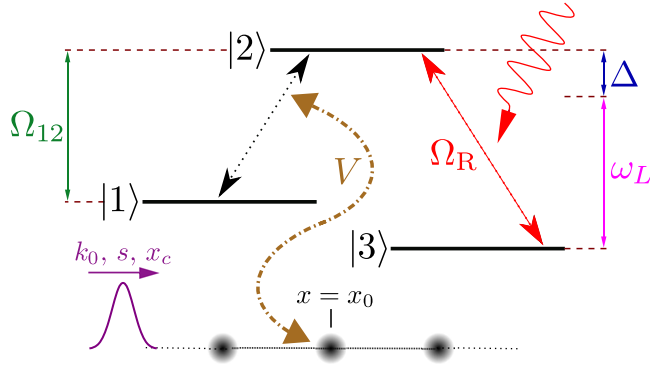$$|\text{atom}\rangle_{\text{photon transmitted}} = t_{k1}|1\rangle + t_{k3}|3\rangle. \tag{35}$$

Figure 7. Illustration of the waveguiding system with a side coupled driven Λ-system. The transition between the states $|3\rangle$ and $|2\rangle$ is driven by a classical time harmonic electric field that couples to the transition with a strength described by the Rabi frequency Ω_R. The frequency of the driving field is detuned to the transition energy by a value of Δ. The remaining notations are the same as those in figures 1 and 4.

In figure 6, we display the transmittances $|t_{ki}|^2$ and reflectances $|r_{ki}|^2$ for each channel $i \in \{1, 3\}$ according to (32a)–(32d). Furthermore, we depict in figure 6 the absolute deviations to the corresponding values of $|t_{\text{pulse},i}|^2$ and $|r_{\text{pulse},i}|^2$ that we have obtained from Gaussian wave packet simulations of (21). Here, we have chosen equal coupling strengths $V_1 = V_3 = J$, so that the reflection amplitudes (32a) and (32c) are identical. Therefore, if a reflected photon is detected, the relative phase factor $\exp(i\Delta\varphi)$ in (33) becomes unity. This results in an equal superposition of the two lower atomic states which are then in phase.

As a result of the atomic superposition being in phase, figure 6 demonstrates that now a second photon with $\epsilon_k = \Omega_{12}$ would be reflected completely—and this is independent of the energy of the first reflected photon. The atom acting as a perfect mirror is well known from similar systems where 2LS [9] or V-systems [27] serve as quantum impurities. However, as our above discussion demonstrates, for an undriven Λ-system, this behavior can only occur in a TCC.

If a transmitted photon is detected, figure 6 demonstrates that the resulting atomic state after scattering strongly depends on the initial relative phase in (33). Even though both transmittances $|t_{ik}|^2$ exhibit maxima, after scattering the atomic state remains in a superposition of both lower states.

4. Single-photon transport through driven three-level system

4.1. Transmittance through a driven Λ-system

The Hamiltonian of a free but driven Λ-atom in the rotating-wave approximation and in a co-rotating frame reads (cf [27] and figure 7)

$$\hat{H}_A = E_1|1\rangle\langle 1| + (E_1 + \Omega_{12})\,|2\rangle\langle 2| + (E_1 + \Omega_{12} - \Delta)\,|3\rangle\langle 3| + \frac{\Omega_R}{2}\,(|3\rangle\langle 2| + |2\rangle\langle 3|)\,. \tag{36}$$

Here, Δ is the detuning between the driving field and the energy of the driven transition. The Rabi frequency is denoted by Ω_R. This Hamiltonian can be diagonalized, i.e.

$$\hat{H}_A = E_1 |1\rangle\langle 1| + E_+ |+\rangle\langle +| + E_- |-\rangle\langle -|, \tag{37}$$

with the new dressed states

$$|\pm\rangle = \frac{1}{\sqrt{2\Omega_{eff}(\Omega_{eff} \mp \Delta)}} \left(\Omega_R |2\rangle - (\Delta \mp \Omega_{eff})|3\rangle\right), \tag{38}$$

and their corresponding eigenvalues are

$$E_\pm = E_1 + \Omega_{12} - \frac{1}{2}\left(\Delta \mp \Omega_{eff}\right). \tag{39}$$

Further, the effective Rabi frequency is denoted by

$$\Omega_{eff} = \sqrt{\Delta^2 + \Omega_R^2}. \tag{40}$$

In this dressed-state basis, the interaction Hamiltonian $\hat{H}_I = V(|1\rangle\langle 2|\hat{a}_{x_0} + \text{h.c.})$ then reads as

$$\hat{H}_I = \sum_{i=+,-} V_i \left(|i\rangle\langle 1|\hat{a}_{x_0} + \text{h.c.}\right), \tag{41}$$

where the new coupling strengths are

$$V_\pm = \frac{V\Omega_{eff}}{\sqrt{2\Omega_{eff}(\Omega_{eff} \mp \Delta)}}. \tag{42}$$

Obviously, equation (41) has the same form as (8). Thus, the side-coupled driven Λ-system in the dressed-basis representation maps onto an undriven V-system with eigenenergies $E_\pm$ and coupling strengths $V_\pm$ depending on the detuning Δ and the Rabi frequency Ω_{eff} of the driving field (cf [27]). For a plane-wave state, the reflection coefficient r in the stationary regime is determined by

$$r = \frac{-2iV^2(\Delta + \epsilon_k - \Omega_{12})}{2iV^2(\Delta + \epsilon_k - \Omega_{12}) + J\sin(k)(4(\epsilon_k - \Omega_{12})(\Delta + \epsilon_k - \Omega_{12}) - \Omega_R^2)}. \tag{43}$$

As calculated in [27] for a linearized dispersion relation, the reflection coefficient (43) vanishes in the case of two-photon resonance, i.e. $\epsilon_k = \Omega_{12} - \Delta$, which is also the case in the present system. In other words, this is a realization of EIT for a single photon and a single atom.

In figure 8, we depict the analytically calculated reflectance $|r|^2$ and a comparison to numerical simulations that use Gaussian single-photon pulses. For the pulses, the EIT effect is not as strong as it is in the case of a monochromatic plane wave, which again, is a result of the non-vanishing spectral width of the pulse.

4.2. Momentum transfer in a driven V-system

Similar to the driven Λ-system, the Hamiltonian of a driven V-system reads in the rotating-wave approximation and in a co-rotating frame (cf [27] and figure 9)

$$\begin{aligned}\hat{H}_A &= (E_2 + \Omega_{21})|1\rangle\langle 1| + E_2|2\rangle\langle 2| + (E_2 + \Delta)|3\rangle\langle 3| + \frac{\Omega_R}{2}\left(|3\rangle\langle 2| + |2\rangle\langle 3|\right), \\ &= (E_2 + \Omega_{21})|1\rangle\langle 1| + E_+|+\rangle\langle +| + E_-|-\rangle\langle -|. \end{aligned} \tag{44}$$
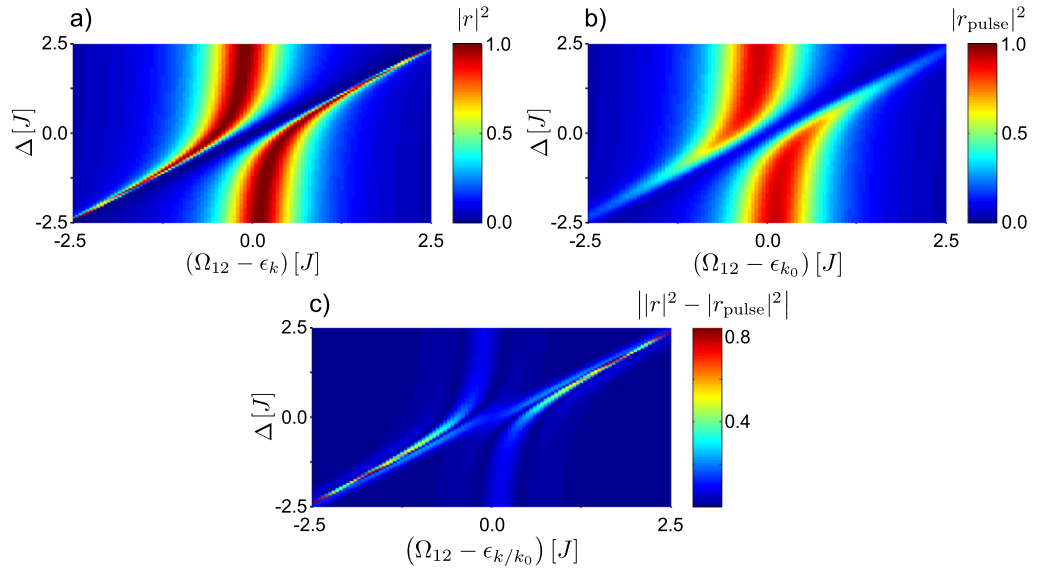
Figure 8. Analytical transmittances $|r|^2$ for plane-wave states with $k = \pi/2$ (panel (a)), corresponding simulated transmittances $|r_{\text{pulse}}|^2$ for a Gaussian pulse with $k_0 = \pi/2$ (panel (b)), absolute difference between the simulation and the analytical calculation (panel (c)). The full transmittance (EIT) in case of the two-photon resonance (main diagonal in panel (a)) is not perfect in the simulation due to the finite spectral width of the Gaussian pulse. The parameters of the simulations are $V = \Omega_R = J$, $\Omega_{12} = \epsilon_{k_0}$, $s = 9$, $x_c = 420$ and the waveguide consists of 999 real-space sites.
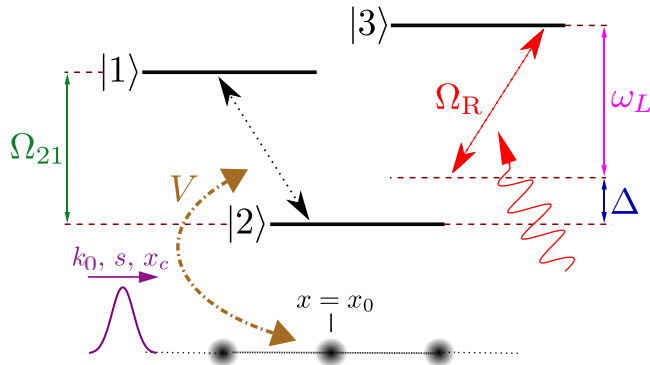

Figure 9. Parameters in systems with a side coupled driven Λ-system. The parameters are denoted in the same way as in figure 7.

The corresponding dressed eigenstates $|+\rangle$ and $|-\rangle$ are

$$|\pm\rangle = \frac{1}{\sqrt{2\Omega_{\text{eff}}(\Omega_{\text{eff}} \pm \Delta)}} \left(\Omega_R|2\rangle + (\Delta \pm \Omega_{\text{eff}})|3\rangle\right), \qquad (45)$$

and the new eigenvalues E_+ and E_- read

$$E_\pm = E_2 + \frac{1}{2}\left(\Delta \pm \Omega_{\text{eff}}\right), \qquad (46)$$

where the effective Rabi frequency Ω_{eff} is identical to that of section 4.1. Consequently, the Hamiltonian $\hat{H}_{\text{I}}$ describing the interaction of the waveguide modes and the atom reads

$$\hat{H}_{\text{I}} = \sum_{i=+,-} V_i(|1\rangle\langle i|\hat{a}_{x_0} + \text{h.c.}), \tag{47}$$

where the coupling strengths are

$$V_{\pm} = \frac{V\Omega_{\text{eff}}}{\sqrt{2\Omega_{\text{eff}}(\Omega_{\text{eff}} \pm \Delta)}}. \tag{48}$$

Equation (47) is of the same form as (18). Hence, the driven V-system is mapped to an undriven Λ-system. As in section 4.1, the eigenenergies and coupling strengths depend on the detuning Δ and the Rabi frequency Ω_{R}.

The fact that a driven V-system effectively behaves like an undriven Λ-system implies that we need to consider all possible initial conditions of an undriven Λ-system, for instance, OCCs or TCCs. The two lower states of the mapped driven V-system are the states $|+\rangle$ and $|-\rangle$. In general, the initial state of the atom is a superposition of the states $|+\rangle$ and $|-\rangle$ in turn, this superposition can be controlled and prepared experimentally by techniques such as STIRAP [20].

In the following, we do not address the problem of the atomic state preparation and restrict our investigation to the OCCs. We assume that the atom, without the loss of generality, is initially in state $|+\rangle$. According to (46), the two transition energies of the mapped Λ-system read

$$\Omega_{\pm 1} = E_1 - E_{\pm} = \Omega_{21} - \frac{1}{2}(\Delta \pm \Omega_{\text{eff}}). \tag{49}$$

Let k_+ be a wavenumber of a photon, which is absorbed in the channel of state $|+\rangle$. Then, the wavenumber that corresponds to a photon scattered into the channel of state $|-\rangle$ is determined by

$$\epsilon_{k_-} = \epsilon_{k_+} + \Omega_{-1} - \Omega_{+1}. \tag{50}$$

This is a consequence of energy conservation. Upon combining (50) and (49), we obtain

$$k_- = -\text{i}\ln\left(\gamma \pm \sqrt{\gamma^2 - 1}\right), \tag{51}$$

where

$$\gamma = \cos(k_+) - \frac{\Omega_{\text{eff}}}{2J}. \tag{52}$$

The signs in (51) distinguish between the cases where k_- belongs to either a transmitted (plus) or to a reflected wave (minus).

In figure 10, we display the dependence of k_- on γ. If $\gamma \leqslant -1$, k_- is complex with a constant real part $\text{Re}(k_-) = \pi$. In this case, the radiation emitted into the channel of state $|3\rangle$ cannot propagate in the waveguide, gets reabsorbed and emitted into the channel of state $|1\rangle$. Hence, the atom will be in state $|+\rangle$ after scattering. This effect can be enhanced to an extreme by increasing the effective Rabi frequency Ω_{eff} to $\Omega_{\text{eff}} \geqslant 4J$. In this case, the atom will stay in state $|+\rangle$ after scattering independent of the wavenumber k_+ of the incoming photon. This effect is attributed to the existence of band edges and band gaps in the dispersion relation of the waveguide and cannot occur in waveguiding systems whose spectrum is unbound.
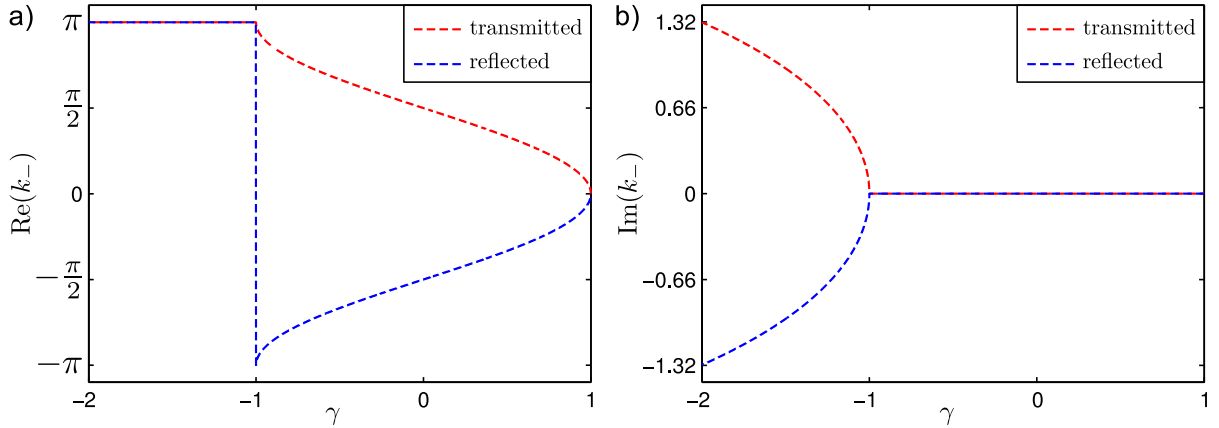
Figure 10. Real part (panel (a)) and imaginary part (panel (b)) of the wavenumber k_- as a function of the parameter γ in (51). The red lines correspond to right moving and, therefore, transmitted waves, whereas the blue lines correspond to left moving and, therefore, reflected waves.
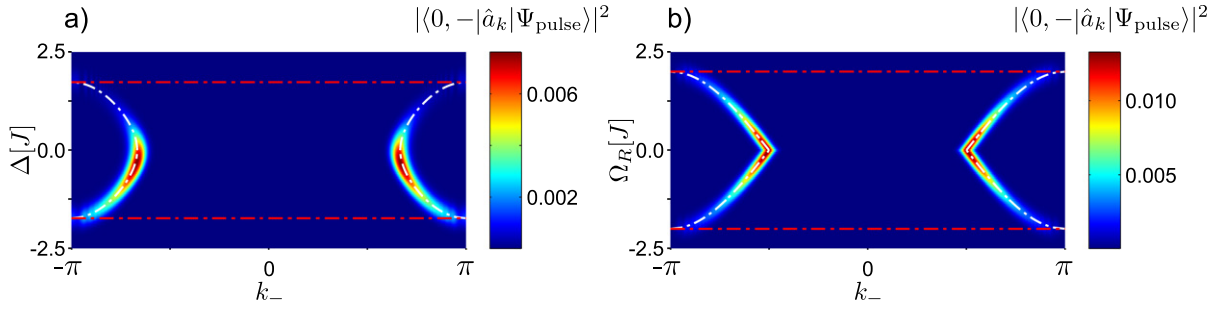

Figure 11. Occupation of momentum space in channel '$-$' after scattering by varying the detuning Δ (panel (a)) and the Rabi frequency Ω_R (panel (b)) of a time-domain simulation for a single-photon pulse and the corresponding wavenumbers calculated from (51) (white dashed lines). Note the cut off due to the finite bandwidth of the waveguide (red dashed lines). The parameters of the simulation are (a) $\Omega_R = V = J$, $\Omega_{21} = \epsilon_{k_0}$, $k_0 = \pi/2$, $s = 9$, $x_c = 420$ and (b) $\Delta = 0$, $V = J$, $\Omega_{21} = \epsilon_{k_0}$, $k_0 = \pi/2$, $s = 9$, $x_c = 420$ and the waveguide consists of 999 real-space sites.

In figure 11, we display the photon's momentum distribution in the channel of state $|-\rangle$, i.e. $|\langle 0, -|\hat{a}_k|\Psi_{\text{pulse}}\rangle|^2$, as a function of Δ and Ω_R, respectively. The state $|\Psi_{\text{pulse}}\rangle$ is a Gaussian pulse of the form (20). The ladder operators $\hat{a}_k$ in momentum space are related to those in real space via a lattice Fourier transform [10]. We clearly observe the region where the emission into the channel of state $|-\rangle$ is forbidden—as noted above, this is a result of the finite bandwidth of the waveguide's dispersion relation.

5. Conclusion

In conclusion, we have investigated the single-photon transport properties in a 1D waveguide with an embedded three-level quantum impurity. In such systems, the wavepacket dynamics in

the case of the V-type quantum impurity exhibits the striking feature of long-time occupations of the upper atomic levels. We have shown that this originates in the excitation of *almost* dark states in systems where the upper atomic levels are slightly detuned. Further, we have shown that this effect also occurs in a simplified *poor man's model*, where we have replaced the waveguide by a leaky cavity. Hence, this effect should be independent of the actual kind of waveguide the V-type quantum impurity is embedded in. In turn, this effect might, therefore, find applications in the field of all-optical buffers.

In contrast to a V-atom, a Λ-type three-level quantum impurity embedded in a waveguide supports non-stationary dark states. Furthermore, in the case of TCC and the impurity being in an equal superposition of its degenerate lower states, we have shown that the scattering characteristics depend strongly on the relative phase between these lower states. This may be exploited to characterize the fidelity of preparing a specific state of a 3LS with a prescribed relative phase.

For driven 3LS, we have found that a transmittance of unity due to an EIT of single photons cannot be fully realized by a single-photon pulse because of its finite spectral width. We have further shown how the finite bandwidth of a waveguide's dispersion relation influences the scattering properties of driven systems and how a change in the driving field's parameters affects both the quantum impurity's and the photon's states after scattering.

Acknowledgments

References

[1] You J Q and Nori F 2011 Atomic physics and quantum optics using superconducting circuits *Nature* **474** 589–97

[2] Houck A A, Tureci H E and Koch J 2012 On-chip quantum simulation with superconducting circuits *Nature Phys.* **8** 292–9

[3] Santori C, Fattal D and Yamamoto Y 2010 *Single-Photon Devices and Applications* (Berlin: Wiley)

[4] Benson O 2011 Assembly of hybrid photonic architectures from nanophotonic constituents *Nature* **480** 193–9

[5] Laucht A *et al* 2012 A waveguide-coupled on-chip single-photon source *Phys. Rev. X* **2** 011014

[6] Shadbolt P J, Verde M R, Peruzzo A, Politi A, Laing A, Lobino M, Matthews J C F, Thompson M G and O'Brien J L 2012 Generating, manipulating and measuring entanglement and mixture with a reconfigurable photonic circuit *Nature Photon.* **6** 45–9

[7] Shen J T and Fan S 2005 Coherent photon transport from spontaneous emission in one-dimensional waveguides *Opt. Lett.* **30** 2001–3

[8] Shen J T and Fan S 2005 Coherent single photon transport in a one-dimensional waveguide coupled with superconducting quantum bits *Phys. Rev. Lett.* **95** 213001

[9] Zhou L, Gong Z R, Liu Y X, Sun C P and Nori F 2008 Controllable scattering of a single photon inside a one-dimensional resonator waveguide *Phys. Rev. Lett.* **101** 100501

[10] Longo P, Schmitteckert P and Busch K 2009 Dynamics of photon transport through quantum impurities in dispersion-engineered one-dimensional systems *J. Opt. A: Pure Appl. Opt.* **11** 114009

[11] Shen J T and Fan S 2007 Strongly correlated two-photon transport in a one-dimensional waveguide coupled to a two-level system *Phys. Rev. Lett.* **98** 153003

[12] Shen J T and Fan S 2007 Strongly correlated multiparticle transport in one dimension through a quantum impurity *Phys. Rev.* A **76** 062709

[13] Zheng H, Gauthier D J and Baranger H U 2010 Waveguide QED: many-body bound-state effects in coherent and Fock-state scattering from a two-level system *Phys. Rev.* A **82** 063816

[14] Longo P, Schmitteckert P and Busch K 2010 Few-photon transport in low-dimensional systems: interaction-induced radiation trapping *Phys. Rev. Lett.* **104** 023602

[15] Longo P, Schmitteckert P and Busch K 2011 Few-photon transport in low-dimensional systems *Phys. Rev.* A **83** 063828

[16] Rephaeli E and Fan S 2012 Stimulated emission from a single excited atom in a waveguide *Phys. Rev. Lett.* **108** 143602

[17] Baragiola B Q, Cook R L, Brańczyk A M and Combes J 2012 *n*-photon wave packets interacting with an arbitrary quantum system *Phys. Rev.* A **86** 013811

[18] Longo P, Cole J H and Busch K 2012 The Hong–Ou–Mandel effect in the context of few-photon scattering *Opt. Express* **20** 12326–40

[19] Fleischhauer M, Imamoglu A and Marangos J P 2005 Electromagnetically induced transparency: optics in coherent media *Rev. Mod. Phys.* **77** 633–73

[20] Bergmann K, Theuer H and Shore B W 1998 Coherent population transfer among quantum states of atoms and molecules *Rev. Mod. Phys.* **70** 1003–25

[21] Abdumalikov A A, Astafiev O, Zagoskin A M, Pashkin Yu A, Nakamura Y and Tsai J S 2010 Electromagnetically induced transparency on a single artificial atom *Phys. Rev. Lett.* **104** 193601

[22] Astafiev O V, Abdumalikov A A, Zagoskin A M, Pashkin Yu A, Nakamura Y and Tsai J S 2010 Ultimate on-chip quantum amplifier *Phys. Rev. Lett.* **104** 183603

[23] Chang D E, Sorensen A S, Demler E A and Lukin M D 2007 A single-photon transistor using nanoscale surface plasmons *Nature Phys.* **3** 807–12

[24] Gong Z R, Ian H, Zhou L and Sun C P 2008 Controlling quasibound states in a one-dimensional continuum through an electromagnetically-induced-transparency mechanism *Phys. Rev.* A **78** 053806

[25] Kolchin P, Oulton R F and Zhang X 2011 Nonlinear quantum optics in a waveguide: distinct single photons strongly interacting at the single atom level *Phys. Rev. Lett.* **106** 113601

[26] Tsoi T S and Law C K 2009 Single-photon scattering on λ-type three-level atoms in a one-dimensional waveguide *Phys. Rev.* A **80** 033823

[27] Witthaut D and Sørensen A S 2010 Photon scattering by a three-level emitter in a one-dimensional waveguide *New J. Phys.* **12** 043052

[28] Roy D 2011 Two-photon scattering by a driven three-level emitter in a one-dimensional waveguide and electromagnetically induced transparency *Phys. Rev. Lett.* **106** 053601

[29] Zheng H, Gauthier D J and Baranger H U 2012 Strongly correlated photons generated by coupling a three- or four-level system to a waveguide *Phys. Rev.* A **85** 043832

[30] Busch K, Blum C, Graham A M, Hermann D, Köhl M, Mack P and Wolff C 2011 The photonic Wannier function approach to photonic crystal simulations: status and perspectives *J. Mod. Opt.* **58** 365–83